

# Galaxy Morphology Classification using Neural Ordinary Differential Equations

Raghav Gupta<sup>a</sup>, P.K. Srijith<sup>a</sup>, Shantanu Desai<sup>b</sup>

<sup>a</sup>*Department of Computer Science and Engineering, IIT Hyderabad, Kandi, Telangana-502285, India*

<sup>b</sup>*Department of Physics, IIT Hyderabad, Kandi, Telangana-502285, India*

## Abstract

We use a continuous depth version of the Residual Network (ResNet) model known as Neural ordinary differential equations (NODE) for the purpose of galaxy morphology classification. We applied this method to carry out supervised classification of galaxy images from the Galaxy Zoo 2 dataset, into five distinct classes, and obtained an accuracy of about 92% for most of the classes. Through our experiments, we show that NODE not only performs as well as other deep neural networks, but has additional advantages over them, which can prove very useful for next generation surveys. We also compare our result against ResNet. While ResNet and its variants suffer problems, such as time consuming architecture selection (e.g. the number of layers) and the requirement of large data for training, NODE does not have these requirements. Through various metrics, we conclude that the performance of NODE matches that of other models, despite using only one-third of the total number of parameters as compared to these other models.

*Keywords:* neural ordinary differential equations, galaxy morphology classification, ResNets

## 1. INTRODUCTION

The problem of determining the morphology of a galaxy plays a pivotal role in a large number of fields from galaxy evolution to cosmology. Some of these applications include stellar masses (Bundy et al., 2005), star formation history (Kennicutt, 1998), color (Skibba et al., 2009), gas and dust content (Lianou et al., 2019), age of the galaxy (Bernardi et al., 2010), various dynamical processes (Romanowsky and Fall, 2012), tests of modified gravity theories (Desmond and Ferreira, 2020) etc. A recent review on various aspects of galaxy morphology and its connections to the rest of astrophysics can be found in Buta (2013).

The very first morphological classification schemes pioneered by Hubble (1926) were based upon visual scanning of galaxies and classifying them into different types such as spirals, ellipticals, lenticulars. With the advent of large area optical surveys, the task of visual classification was outsourced to the Galaxy Zoo project (Lintott et al., 2008). The first incarnation of the project (Galaxy Zoo 1), consisting of a dataset of more than 900,000 images by the Sloan Digital Sky Survey (York et al., 2000), was classified by citizen scientists into four categories: “spiral”, “elliptical”, “a merger” or “star/don’t know” (Lintott et al., 2008). The project enabled the annotation of a million galaxy images within several months. This was superseded by Galaxy Zoo 2 (Willett et al., 2013), Galaxy Zoo: Hubble (Willett et al., 2017), and Galaxy Zoo: CANDELS (Simmons et al., 2017).

Unfortunately, this manual approach of visual classification does not scale well with the unprecedented pace of data growth

due to the large number of meter-class telescopes equipped with multi-CCD imagers, which are continuously been built over the past two decades. Very soon stage IV Dark Energy surveys such as Legacy Survey of Space and Time operated by the Vera Rubin observatory (Abell et al., 2009), Euclid (Laureijs et al., 2011), and Roman Space Telescope (Spergel et al., 2013) are going to produce petabytes worth of data, rendering manual classification impossible.

Therefore, astronomers have turned their sights to automated classification methods. Over the past few decades, a large amount of literature has emerged on these aforementioned methods for measuring galaxy morphology, especially in large observational surveys. These methods range from parametric techniques, which attempt to describe galaxy light profiles using small sets of parameters (Simard et al., 2002; Sersic, 1963; Ode-wahn et al., 2001; Lackner and Gunn, 2012), to non-parametric methods that reduce these light distributions to single values such as in the ‘CAS’ system (Conselice, 2003; Abraham and van den Bergh, 2001; Menanteau et al., 2005), the Gini-M20 coefficients (Freeman et al., 2013), etc. Recent reviews of some of these automated methods can be found in de Diego et al. (2020); Martin et al. (2020).

A major game changer in astronomy and astrophysics has been the widespread application of machine learning and deep learning techniques to a wide variety of problems in astrophysics (Ball and Brunner, 2010; Kremer et al., 2017; Bethapudi and Desai, 2018; Baron, 2019), and galaxy morphology is no exception to this. Applications of machine learning as well as deep learning to galaxy morphology classifications are discussed in Dieleman et al. (2015); Tanoglidis et al. (2020); Tuccillo et al. (2017); Barchi et al. (2020); Khan et al. (2019); Spindler et al. (2020)

Deep learning models, known as deep neural networks

*Email addresses:* cs19mtech11024@iith.ac.in (Raghav Gupta), srijith@iith.ac.in (P.K. Srijith), shantanud@phy.iith.ac.in (Shantanu Desai)

(DNN), have been widely used for image classification and slowly began to beat human accuracy in these tasks, as soon as large training sets started becoming available (Le-Cun et al., 2015). DNN models, especially Convolution Neural Networks (CNN) (Krizhevsky et al., 2012), AlexNet, VGGNet and GoogleNet, took the accuracy of DNNs to new heights. With the advent of Residual Networks (ResNet) (He et al., 2015), researchers were able to make these CNN models deeper than ever before, without suffering from additional problems. Among the machine learning techniques, convolution neural networks (CNN) (Krizhevsky et al., 2012) have become the mainstream method for image classification. However, CNN with a large number of layers suffer from the vanishing gradient problem (Kolen and Kremer, 2001).

In the popular deep learning models such as ResNets, the selection of architecture (depth of the network) and the presence of a large number of parameters can make the training process computationally intractable. Recently, a continuous depth counterpart to ResNets, known as NODE (Chen et al., 2018) were introduced, which could overcome these drawbacks. In our work, we propose to use NODE for the galaxy morphology classification problem. We compare its performance against ResNet, which has also been used in other works (Zhu et al., 2019; Goddard and Shamir, 2020), as that is the state-of-the-art deep learning approach for galaxy morphology classification and demonstrate the benefits of NODE over ResNets.

NODE is inspired by the way ResNet works, where one models the change in the feature maps over layers using a neural network. This can be seen equivalent to an ordinary differential equation with the derivative modelled as a neural network function. Consequently, the final layer feature map can be obtained using numerical solvers for ODE such as Eulers method and Runga-kutta method. NODE has certain advantage over ResNet. In NODE, the network depth is a parameter, rather than being fixed (like in ResNet). Thus, by tuning the depth parameter, we can trade-off between model speed and model accuracy. Another advantage of NODE over ResNet is that, the number of parameters in NODE is much less than ResNet. Models with less number of parameters require less data to train and do not suffer from over-fitting issues.

The NODE architecture has been applied to a wide variety of fields, ranging from biomedical-imaging, high-energy physics, image and video processing, 3D modelling, economics (Groha et al., 2020) etc. For example, in case of biomedical-imaging, it has been used for kidney segmentation (Valle et al., 2019), reconstruction of MRI images (Chen et al., 2020), multi-state survival analysis (Groha et al., 2020) etc. It is also used in the 3-D modelling for accurate manifold generation (Gupta and Chandraker, 2020). It is used for small-footprint keyword spotting (KWS) in audio files (Fuketa and Morita, 2020). In the domain of theoretical High-Energy Physics, it has been applied to holographic QCD problem (Hashimoto et al., 2020). It has also been used to model better systems for mechanical systems (Roehrl et al., 2020). To the best of our knowledge, this technique has not been applied to any problem in astrophysics.

The organization of this manuscript is as follows. In Section 2, we describe the dataset used to carry out our experiments.

Next, we shed some light on ResNet in Section 3, followed by in-depth explanation of working of NODE (Section 4). Thereafter, we explain how we build up data-processing pipeline. We describe the various pre-processing steps applied to the data, followed by exact network architecture used in Section 5. Further, in Section 6, we discuss our experimental results and take help of various tables and diagrams to do so. Finally, we conclude in Section 7.

## 2. DATASET

The dataset used in our experiments is drawn from the Galaxy Zoo Challenge, available on kaggle. Classification labels for the kaggle Dataset (KD) are drawn from Galaxy Zoo 2, and images used are obtained from SDSS-DR7 (Abazajian et al., 2009). Galaxy images used in this dataset are classified into total five classes viz. spiral, edge-on, cigar-shaped smooth, in-between smooth, and completely round smooth. The different morphological types are shown in Fig. 1. Similar to Zhu et al. (2019), we shall use the numerical labels 0,1,2,3,4 to annotate completely round, in-between, cigar-shaped, edge-on, and spiral galaxies, respectively.

KD consists of around 60,000 images, and each image is divided into five classes, with a classification probability provided for each class. We prune this dataset further and only select those images, which are classified with high probability in their respective classes. After pruning, 25911 images are selected, with single class assigned to each image.

The selection criteria is similar to that described in Willett et al. (2013), in which galaxy images classified with, probabilities higher than a certain threshold (discussed therein), are selected. After these cuts, we have 7806, 3903, 578, 8069, and 8434 images in each class, in the order listed at the beginning of this section.

The size of each image is  $424 \times 424 \times 3$  pixels, where the last dimension denotes the number of colour channels viz. RGB. The galaxy of interest is generally located at the center of the image. We finally split in our data in ratio of 9:1 for the purpose of training and testing, thus assigning 25911 and 2879 galaxies, respectively for each task.

## 3. Residual Neural Networks

Neural networks are modelled as a series of transformations with discrete number of layers, with each one taking in a previous hidden representation  $\mathbf{h}_l$  and producing a new hidden representation  $\mathbf{h}_{l+1} = F^l(\mathbf{h}_l)$ . We typically consider the transformation as  $F(\mathbf{x}) = \sigma(\sum_i W_i x_i)$ , where  $\sigma$  is an activation function (e.g. RELU or a sigmoid), and  $\theta$  is a collection of weight vectors. Recently, many deep learning models were introduced based on the idea that increasing the number of layers can improve the performance. However, this may lead to problems such as vanishing gradients (Kolen and Kremer, 2001), where the initial layer weight vectors cannot be computed correctly through back propagation as the error gradient becomes small.

This problem was addressed by Deep Residual Learning (He et al., 2015). ResNets are a class of DNNs, which try to map

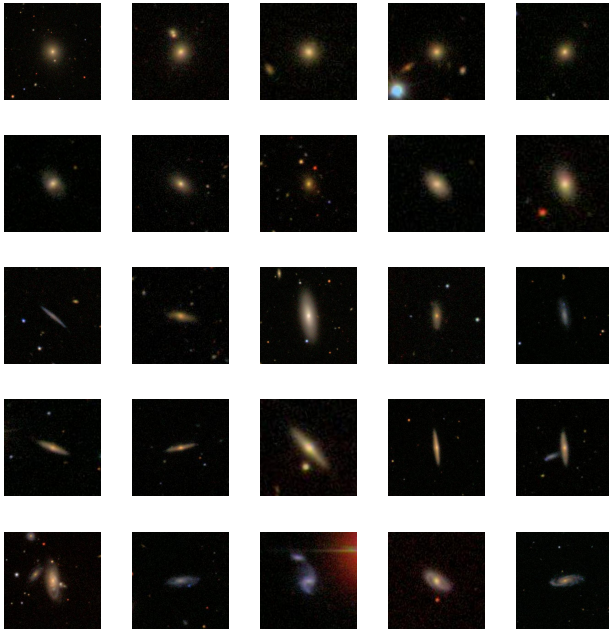


Figure 1: The five different galaxy morphologies in the Galaxy Zoo -2 dataset. These classes are completely round smooth, in-between smooth, cigar-shaped smooth, edge-on and spiral, from top to bottom. See also Fig. 1 of [Zhu et al. \(2019\)](#) for more examples of different galaxy morphologies from this dataset.

residuals instead of complete transformation itself in the hidden layer mappings. The idea is to learn a mapping as the difference between layers (or equivalently adding skip connections):  $\mathbf{h}_{l+1} = F^l(\mathbf{h}_l) + \mathbf{h}_l$ . In [He et al. \(2015\)](#), they showed that this simple transformation avoids the vanishing gradient problem due to skip connections and the networks can learn the weights properly. This allowed the development of deep learning models with a large number of layers (e.g. ResNet with 50 and 100 layers)

ResNet and its variants were able to achieve state-of-art results for image classification. ResNet, proposed by researchers at Microsoft Research, won the ILSVRC challenge in 2015. Many other variants of ResNet, achieved state-of-the-art (SOTA) results in other image datasets. ResNet mainly had two types of residual blocks. In the standard block, two  $3 \times 3$  convolutions are applied, along with a skip connection. In another block, known as the bottleneck block,  $1 \times 1$  convolutions are applied before and after the  $3 \times 3$  convolutions, in order to reduce feature space, so that computation complexity is reduced.

## 4. Neural Ordinary Differential Equations

### 4.1. Euler's method and residual networks

Recently, [Chen et al. \(2018\)](#); [Lu et al. \(2017\)](#) have shown that continuous depth ResNets, known as NODE, can be developed by relating them to ordinary differential equations. Assuming the mapping function to be the same across all the layers, and let  $\Delta t \in \mathbb{R}$ , we can rewrite the hidden representation update of

ResNets as state updates at some time  $t$ .

$$\mathbf{h}(t+1) = F(\mathbf{h}(t)) + \mathbf{h}(t) = \frac{\Delta t}{\Delta t} F(\mathbf{h}(t)) + \mathbf{h}(t) = \Delta t G(\mathbf{h}(t)) + \mathbf{h}(t) \quad (1)$$

where  $G(\mathbf{h}(t)) = F(\mathbf{h}(t))/\Delta t$ . This reformulation is the same as the single step of Euler's method for solving ordinary differential equations of the form as observed in [Lu et al. \(2017\)](#).

$$\frac{d\mathbf{h}(t)}{dt} = G(\mathbf{h}(t), t, \theta) \quad (2)$$

As compared to standard differential equations, the derivative is represented by a function parameterized using a neural network  $G$  acting on the state  $\mathbf{h}(t)$ . Here, we have assumed  $G$ 's to depend on  $t$  as well as some parameters  $\theta$  (parameters of the neural network). One can consider advances in the neural network models considering the convolution operation to represent the mapping  $G$  when applied to image data. Considering Eq. (1), the final representation (feature map) of our network is the state  $\mathbf{h}(T)$  at time  $T$ . This is then fed to a fully-connected neural network (FCNN) to predict the final output which is a real value for regression problems and a discrete value for classification. For a neural network function  $G$ , we can use any off-the-shelf ODE solvers such as Euler's method to solve and obtain the final representation in an iterative manner.

$$\mathbf{h}(T) = \text{ODESolve}(\mathbf{h}(t_0), G, t_0, T, \theta)$$

There is a large amount of research on different methods that can be used to solve ODE. In addition to Eulers method, one could use higher order methods such as Runge-Kutta (RK4) and methods with adaptive step-size.

### 4.2. Training Process

Training a NODE involves learning the parameters of the neural network function using an appropriate loss function (cross entropy in the case of classification). The representation learnt using an ODE solver is fed to the loss function which is optimized with respect to the parameters  $\theta$

$$\arg \min_{\theta} L(\mathbf{h}(T)) = \arg \min_{\theta} L(\text{ODESolve}(\mathbf{h}(t_0), G, t_0, t_1, \theta))$$

The learning of the parameters requires back-propagating through the solver by taking gradients with respect to the loss and this is computationally costly using the naive back-propagation. [Chen et al. \(2018\)](#) proposed an adjoint sensitivity method to learn the parameters by running another ODE solver backward in time.

To optimize  $L$  and learn parameters  $\theta$ , we require gradients with respect to  $\mathbf{h}(t)$  (the state of our system at any time  $t$ ), and  $\theta$  the neural network parameters. The adjoint method describes a way to efficiently compute the derivative of the loss with respect to the state. In brief, we define the adjoint state as

$$a(t) = -\partial L / \partial \mathbf{h}(t)$$

which describe the gradient of the loss with respect to some state  $\mathbf{h}(t)$ . It turns out that the dynamics of the adjoint state can be

described using another ODE.

$$\frac{da(t)}{dt} = -a(t)^T \frac{\partial G(\mathbf{h}(t), t, \theta)}{\partial \mathbf{h}} \quad (3)$$

The gradient of the loss at the initial state  $a(t_0)$  can be computed by running (3) in the backwards direction with initial value as  $a(T)$ . We can compute the derivative of  $G$  with respect to  $\mathbf{h}$  easily: gradient computed through back-propagation in traditional neural networks. Now, the gradient of the loss with respect to parameters  $dL/d\theta$  can be computed as

$$\frac{dL}{d\theta} = - \int_{t_0}^T a(t)^T \frac{\partial G(\mathbf{h}(t), t, \theta)}{\partial \theta} dt$$

The approach known as adjoint sensitivity has better memory cost, linear scalability and low numerical instabilities.

## 5. EXPERIMENTAL SETUP

### 5.1. Network Architecture

The network architecture used for NODE training is as follows. We use a standard convolution block, consisting of two CLN (Convolution, Non-Linearity, Normalization) layers. Each convolution is  $3 \times 3$  convolution.

We also down-sample the input, before passing it to the ODE network. Down-sampling consists of applying 2D convolutions, while reducing the number of channels. Once the input is down-sampled, it passes from the above ODE network, followed by a pooling layer. ODE maps the inputs to some desired latent space, which has the same number of dimensions as input. Similar to a classification task, as our final output has 5 dimensions (equal to the number of classes), we use fully connected layer at the end. This FC layer learns a linear mapping from the ODE output to the final output.

For ResNet, we use two NLC (Normalization, Non-Linearity, Convolution) layers for the architecture, instead of CLN layers (as in NODE). This is also referred as Pre-Activation (as the ReLU operation is carried before convolution). The convolution operation used here is again  $3 \times 3$  convolution. Finally, the output from these layers is added to original input (thus these layers only learn the residual). This constitutes one residual block. We take six such blocks, back to back, to form our ResNet. As mentioned above, down-sampling is applied before this network, followed by pooling operation and FC layer at the end.

### 5.2. Preprocessing

Standard image processing is done on our image dataset, before it could be fed into the model. This is done so as to ensure that the images carry relevant information, which helps to train the model well. It also helps to increase the image dataset size, thus leading to better regularization.

We mainly apply three image transformations. First, the image is resized from  $424 \times 424 \times 3$  pixels to  $32 \times 32 \times 3$  pixels, using bilinear interpolation. This makes our training process faster as the number of dimensions in the input image is largely reduced. The transformation applied involves randomly flipping

the image horizontally. The final transformation involves image normalization, where all the three channels are normalized according to appropriate values. The data set is randomly split into training and testing set in the ratio 9:1 with 25911 images for training set and 2879 images for testing set as discussed in Section 2.

### 5.3. Implementation Details

We use mini-batch gradient descent with a batch size of 256. The initial learning rate is set to 0.1, then decreased by a factor of 10 to 30K and 60K iterations. The weight decay is 0.0001, dropout probability value is 0.8 and the weights are initialized in the same way as in He et al. (2015). It takes about 12 hours to train a single network with on NVIDIA dgx server with P100 GPU.

## 6. RESULTS AND DISCUSSION

### 6.1. Model Accuracy

The model achieves an accuracy of 92.04%, when trained with the Runge-Kutta method and 90% when trained with the Euler method. The accuracy achieved by ResNet on similar architecture is 92.25%. Thus, we can say that NODE achieves similar accuracy as state-of-the-art models like ResNet, while having much lower number of parameters. Table 1 and Table 2 provides the confusion matrix for NODE and ResNet respectively for the different classes. On the whole, the results of the completely round, the in-between, the edge-on and the spiral are extremely excellent, except for the cigar-shaped images. It happens due to the small number of the cigar-shaped images for training.

	0	1	2	3	4
0	777	37	0	2	23
1	19	721	2	2	27
2	0	6	33	20	0
3	0	5	12	374	5
4	11	42	5	13	743

Table 1: Confusion Matrix for NODE, where 0 : Completely round smooth, 1 : In-between smooth, 2 : Cigar-shaped smooth, 3 : Edge-on, and 4 : Spiral.

	0	1	2	3	4
0	796	26	0	0	20
1	37	740	0	0	15
2	1	17	23	19	5
3	0	7	11	356	23
4	11	16	0	15	741

Table 2: Confusion Matrix for ResNet, where 0 : Completely round smooth, 1 : In-between smooth, 2 : Cigar-shaped smooth, 3 : Edge-on, and 4 : Spiral.

### 6.2. Parameters Discussion

ResNet with 6 layers has 0.6 million parameters. NODE on the other hand has total of 0.2 million parameters, for both Euler and Runge-Kutta ODE solving methods. Thus, NODE achieves similar overall accuracy with about one-third of parameters.

### 6.3. Precision, Recall and F1

We compare the precision, recall, and F1 scores of NODE against ResNet. The Precision metric is the ratio of the total truth class observations to the total number of observations labelled positive. Recall tries to quantify what proportion of actual positives is correctly classified. While F1 is the harmonic mean of precision and recall. More detailed definitions of these metrics can be found in [Bethapudi and Desai \(2018\)](#). These three metrics for NODE are shown in Table 3, while those for ResNet are shown in Table 4. We can clearly see that performance of NODE is almost as good as ResNet.

Table 3: Precision, Recall, F1 scores for NODE

	Precision	Recall	F1
0	0.96	0.90	0.92
1	0.92	0.91	0.88
2	0.12	0.31	0.35
3	0.94	0.92	0.89
4	0.92	0.87	0.88

Table 4: Precision Recall F1 for ResNet

	Precision	Recall	F1
0	0.96	0.92	0.93
1	0.91	0.92	0.91
2	0.25	0.23	0.35
3	0.94	0.91	0.91
4	0.94	0.94	0.93

### 6.4. ROC Curve

ROC curve stands for receiver operating characteristic curve. It plots the true positive against false positive rate, and shows how well a model is able to classify. Area under this curve is called AUC. The closer AUC is to one, better is the model in terms of classification. ROC curves for each class, both for NODE (Fig. 2) and ResNet (Fig. 3) are shown. Micro and macro average for all the classes are also shown in the same figures. As we can see, the ROC curves for NODE are very close to those of ResNet for each class. In Fig 4, we plot the average curve (across all classes), both for NODE and ResNet. As we can see, the performance of NODE is competitive compared to ResNet.

## 7. CONCLUSIONS

In this paper, we have used NODE, which is a recently proposed deep learning model, for the task of galaxy morphology classification and also compared its performance with ResNet. The dataset used for this purpose is a subset of Galaxy Zoo 2 dataset. As shown in the results above, the number of parameters in NODE is much less compared to its counterpart ResNet, and it achieves this without compromising the performance. Both models achieve top accuracy of 92%. Also, in NODE, we can easily trade-off accuracy for speed, which is not possible for ResNet. For example, in our experiments, we train NODE with

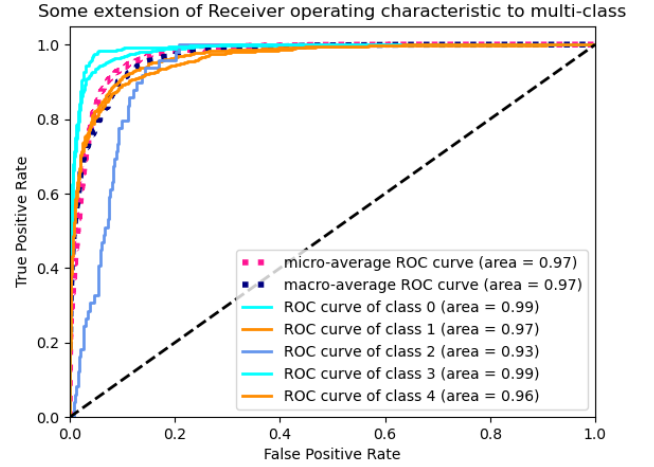


Figure 2: ROC curve for NODE for different classes

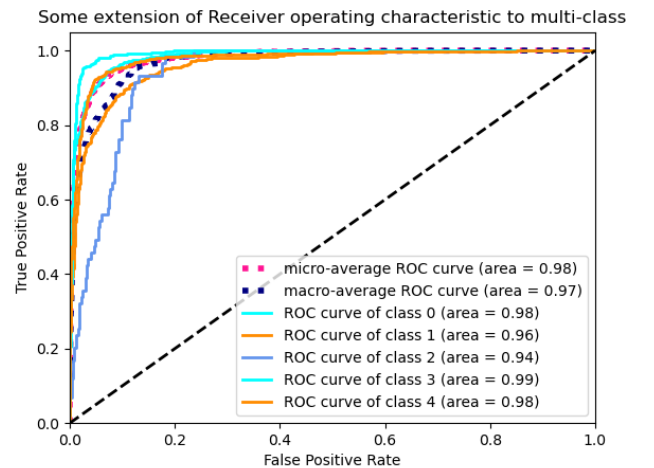


Figure 3: ROC curve for ResNet for different classes.

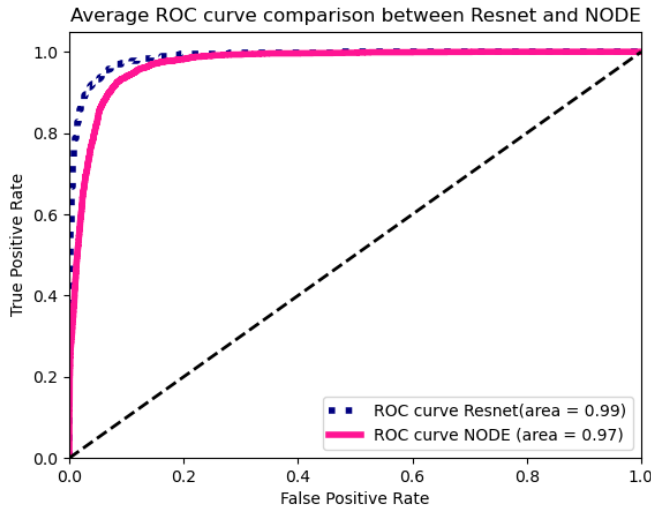


Figure 4: Average ROC curves for ResNet and NODE

two different numerical solvers, viz. Euler and Runge-Kutta. While Euler is much faster than Runge-Kutta, the performance of Runge-Kutta (92%) is better than Euler (90%).

We also compare both the models using other metrics such as precision, recall, F1 and AUC. Through our results, we conclude that, NODE is able to perform as well as ResNet, for all these metrics, while providing all the advantages listed above. We also illustrate this, by plotting the average performance of both NODE and ResNet, on one graph, as shown in Fig 4) above.

From our experiments, we can conclude that NODE can easily replace ResNet, based on the use case. With large scale astronomical surveys coming up, and more and more data being generated from these surveys, it has become a pressing need to replace such classification tasks with robust deep learning models. These emerging deep learning models can not only help to speed-up the process of training and classification, but also provide better insights, by breaking down the process in series of small steps. Thus, researchers have better control over the process, and can easily trade-off one parameter (like accuracy) with another (like speed). We are pretty sure that our methodology would prove very useful for upcoming large scale astronomical surveys such as Vera Rubin LSST, Euclid, WFIRST etc.

## 8. ACKNOWLEDGEMENTS

We would like to thank the galaxy challenge, Galaxy Zoo, SDSS and Kaggle platform for sharing their data. RG is supported by funding from DST-ICPS.

## References

Abazajian, K.N., et al., 2009. The Seventh Data Release of the Sloan Digital Sky Survey. *Astrophys. J. Suppl.* 182, 543–558. [0812.0649](#).

Abell, P.A., et al., 2009. LSST Science Book, Version 2.0 [0912.0201](#).

Abraham, R.G., van den Bergh, S., 2001. The Morphological Evolution of Galaxies. *Science* 293, 1273–1278. [astro-ph/0109358](#).

Ball, N.M., Brunner, R.J., 2010. Data Mining and Machine Learning in Astronomy. *International Journal of Modern Physics D* 19, 1049–1106. [0906.2173](#).

Bamford, S.P., Nichol, R.C., Baldry, I.K., Land, K., Lintott, C.J., Schawinski, K., Slosar, A., Szalay, A.S., Thomas, D., Torki, M., Andreescu, D., Edmondson, E.M., Miller, C.J., Murray, P., Raddick, M.J., Vandenberg, J., 2009. Galaxy zoo: the dependence of morphology and colour on environment. *Monthly Notices of the Royal Astronomical Society* 393, 1324–1352.

Barchi, P.H., de Carvalho, R.R., Rosa, R.R., Sautter, R.A., Soares-Santos, M., Marques, B.A.D., Clua, E., Gonçalves, T.S., de Sá-Freitas, C., Moura, T.C., 2020. Machine and Deep Learning applied to galaxy morphology - A comparative study. *Astronomy and Computing* 30, 100334. [1901.07047](#).

Baron, D., 2019. Machine Learning in Astronomy: a practical overview. *arXiv e-prints* , arXiv:1904.07248 [1904.07248](#).

Bernardi, M., Shankar, F., Hyde, J.B., Mei, S., Marulli, F., Sheth, R.K., 2010. Galaxy luminosities, stellar masses, sizes, velocity dispersions as a function of morphological type. *MNRAS* 404, 2087–2122. [0910.1093](#).

Bethapudi, S., Desai, S., 2018. Separation of pulsar signals from noise using supervised machine learning algorithms. *Astronomy and Computing* 23, 15. [1704.04659](#).

Bundy, K., Ellis, R.S., Conselice, C.J., 2005. The Mass Assembly Histories of Galaxies of Various Morphologies in the GOODS Fields. *ApJ* 625, 621–632. [astro-ph/0502204](#).

Buta, R.J., 2013. Galaxy Morphology. p. 155.

Chen, E.Z., Chen, T., Sun, S., 2020. Mri image reconstruction via learning optimization using neural odes. [2006.13825](#).

Chen, T.Q., Rubanova, Y., Bettencourt, J., Duvenaud, D., 2018. Neural ordinary differential equations. *CoRR* abs/1806.07366. [1806.07366](#).

Conselice, C.J., 2003. The relationship between stellar light distributions of galaxies and their formation histories. [astro-ph/0303065](#).

de Diego, J.A., Nadolny, J., Bongiovanni, Á., Cepa, J., Pović, M., Pérez García, A.M., Padilla Torres, C.P., Lara-López, M.A., Cerviño, M., Pérez Martínez, R., Alfaro, E.J., Castañeda, H.O., Fernández-Lorenzo, M., Gallego, J., González, J.J., González-Serrano, J.I., Pintos-Castro, I., Sánchez-Portal, M., Cedrés, B., González-Otero, M., Heath Jones, D., Bland-Hawthorn, J., 2020. Galaxy classification: deep learning on the OTELO and COSMOS databases. *A&A* 638, A134. [2005.07228](#).

Desmond, H., Ferreira, P.G., 2020. Galaxy morphology rules out astrophysically interesting  $f(R)$ . *arXiv e-prints* , arXiv:2009.08743 [2009.08743](#).

Dieleman, S., Willett, K.W., Dambre, J., 2015. Rotation-invariant convolutional neural networks for galaxy morphology prediction. *MNRAS* 450, 1441–1459. [1503.07077](#).

Dupont, E., Doucet, A., Teh, Y.W., 2019. Augmented neural odes. [1904.01681](#).

E, W., 2017. A proposal on machine learning via dynamical systems. *Communications in Mathematics and Statistics* 5, 1–11.

Freeman, P.E., Izbicki, R., Lee, A.B., Newman, J.A., Conselice, C.J., Koekemoer, A.M., Lotz, J.M., Mozena, M., 2013. New image statistics for detecting disturbed galaxy morphologies at high redshift. [1306.1238](#).

Fuketa, H., Morita, Y., 2020. Neural ode with temporal convolution and time delay neural networks for small-footprint keyword spotting. [2008.00209](#).

Gholami, A., Keutzer, K., Biros, G., 2019. Anode: Unconditionally accurate memory-efficient gradients for neural odes. [1902.10298](#).

Goddard, H., Shamir, L., 2020. A catalog of broad morphology of Pan-STARRS galaxies based on deep learning. *arXiv e-prints* , arXiv:2010.06073 [2010.06073](#).

Groha, S., Schmon, S.M., Gusev, A., 2020. Neural odes for multi-state survival analysis. [2006.04893](#).

Gupta, K., Chandraker, M., 2020. Neural mesh flow: 3d manifold mesh generation via diffeomorphic flows. [2007.10973](#).

Hashimoto, K., Hu, H.Y., You, Y.Z., 2020. Neural ode and holographic qcd. [2006.00712](#).

He, K., Zhang, X., Ren, S., Sun, J., 2015. Deep residual learning for image recognition. *CoRR* abs/1512.03385. [1512.03385](#).

Hubble, E.P., 1926. Extragalactic nebulae. *ApJ* 64, 321–369.

Kennicutt, Robert C., J., 1998. Star Formation in Galaxies Along the Hubble Sequence. *Ann. Rev. of Astronomy and Astrophysics* 36, 189–232. [astro-ph/9807187](#).

Khan, A., Huerta, E.A., Wang, S., Gruendl, R., Jennings, E., Zheng, H., 2019. Deep learning at scale for the construction of galaxy catalogs in the Dark Energy Survey. *Physics Letters B* 795, 248–258. [1812.02183](#).

Kolen, J.F., Kremer, S.C., 2001. Gradient Flow in Recurrent Nets: The Difficulty of Learning LongTerm Dependencies. pp. 237–243.

Kremer, J., Stensbo-Smidt, K., Gieseke, F., Pedersen, K.S., Igel, C., 2017. Big universe, big data: machine learning and image analysis for astronomy. *IEEE Intelligent Systems* 32, 16–22.

Krizhevsky, A., Sutskever, I., Hinton, G.E., 2012. Imagenet classification with deep convolutional neural networks, in: *Advances in Neural Information Processing Systems* 25, pp. 1097–1105.

Krizhevsky, A., Sutskever, I., Hinton, G.E., 2017. ImageNet classification with deep convolutional neural networks. *Communications of the ACM* 60, 84–90.

Lackner, C.N., Gunn, J.E., 2012. Astrophysically motivated bulge-disk decompositions of sdss galaxies. [1201.0763](#).

Lahav, O., Naim, A., Buta, R.J., Corwin, H.G., de Vaucouleurs, G., Dressler, A., Huchra, J.P., van den Bergh, S., Raychaudhury, S., Sodre, L., Storrie-Lombardi, M.C., 1995. Galaxies, Human Eyes, and Artificial Neural Networks. *Science* 267, 859–862. [astro-ph/9412027](#).

Laureijs, R., et al., 2011. Euclid Definition Study Report [1110.3193](#).

LeCun, Y., Bengio, Y., Hinton, G., 2015. Deep learning. *nature* 521, 436–444.

Lianou, S., Barmby, P., Mosenkov, A.A., Lehnert, M., Karczewski, O., 2019. Dust properties and star formation of approximately a thousand local galaxies. *A&A* 631, A38. [1906.02712](#).

Lintott, C.J., Schawinski, K., Slosar, A., Land, K., Bamford, S., Thomas, D., Raddick, M.J., Nichol, R.C., Szalay, A., Andreescu, D., Murray, P., Vandenberg, J., 2008. Galaxy Zoo: morphologies derived from visual inspection of galaxies from the Sloan Digital Sky Survey. *MNRAS* 389, 1179–1189. [0804.4483](#).

Lotz, J.M., Primack, J., Madau, P., 2003. A new non-parametric approach to galaxy morphological classification. [astro-ph/0311352](#).

Lu, Y., Zhong, A., Li, Q., Dong, B., 2017. Beyond finite layer neural networks: Bridging deep architectures and numerical differential equations. [1710.10121](#).

Martin, G., Kaviraj, S., Hocking, A., Read, S.C., Geach, J.E., 2020. Galaxy morphological classification in deep-wide surveys via unsupervised machine learning. *MNRAS* 491, 1408–1426. [1909.10537](#).

McNamara, A., Treuille, A., Popović, Z., Stam, J., 2004. Fluid control using the adjoint method. *ACM Transactions on Graphics* 23, 449.

Menanteau, F., Ford, H.C., Motta, V., Benitez, N., Martel, A.R., Blakeslee, J.P., Infante, L., 2005. The morphological demographics of galaxies in the ahs hubble ultra deep parallel fields. [astro-ph/0509759](#).

Odewahn, S.C., Cohen, S.H., Windhorst, R.A., Philip, N.S., 2001. Automated galaxy morphology: A fourier approach. [astro-ph/0110275](#).

Pedregosa, F., Varoquaux, G., Gramfort, A., Michel, V., Thirion, B., Grisel, O., Blondel, M., Müller, A., Nothman, J., Louppe, G., Prettenhofer, P., Weiss, R., Dubourg, V., Vanderplas, J., Passos, A., Cournapeau, D., Brucher, M., Perrot, M., Édouard Duchesnay, 2012. Scikit-learn: Machine learning in python. [1201.0490](#).

Peth, M.A., Lotz, J.M., Freeman, P.E., McPartland, C., Mortazavi, S.A., Snyder, G.F., Barro, G., Grogin, N.A., Guo, Y., Hemmati, S., Kartaltepe, J.S., Kocevski, D.D., Koekemoer, A.M., McIntosh, D.H., Nayyeri, H., Papovich, C., Primack, J.R., Simons, R.C., 2015. Beyond spheroids and discs: Classifications of candelas galaxy structure at  $1.4 < z < 2$  via principal component analysis. [1504.01751](#).

Roehrl, M.A., Runkler, T.A., Brandstetter, V., Tokic, M., Obermayer, S., 2020. Modeling system dynamics with physics-informed neural networks based on lagrangian mechanics. [2005.14617](#).

Romanowsky, A.J., Fall, S.M., 2012. Angular Momentum and Galaxy Formation Revisited. *ApJS* 203, 17. [1207.4189](#).

Scarlata, C., Carollo, C.M., Lilly, S., Sargent, M.T., Feldmann, R., Kampczyk, P., Porciani, C., Koekemoer, A., Scoville, N., Kneib, J.P., Leauthaud, A., Massey, R., Rhodes, J., Tasca, L., Capak, P., Maier, C., McCracken, H.J., Mobasher, B., Renzini, A., Taniguchi, Y., Thompson, D., Sheth, K., Ajiki, M., Aussel, H., Murayama, T., Sanders, D.B., Sasaki, S., Shioya, Y., Takahashi, M., 2007. COSMOS morphological classification with the zurich estimator of structural types (ZEST) and the evolution since  $z = 1$  of the luminosity function of early, disk, and irregular galaxies. *The Astrophysical Journal Supplement Series* 172, 406–433.

Schawinski, K., Lintott, C., Thomas, D., Sarzi, M., Andreescu, D., Bamford, S.P., Kaviraj, S., Khochfar, S., Land, K., Murray, P., Nichol, R.C., Raddick, M.J., Slosar, A., Szalay, A., Vandenberg, J., Yi, S.K., 2009. Galaxy zoo: a sample of blue early-type galaxies at low redshift. *Monthly Notices of the Royal Astronomical Society* 396, 818–829.

Selim, I.M., Aziz, M.A.E., 2017. Automated morphological classification of galaxies based on projection gradient nonnegative matrix factorization algorithm. *Experimental Astronomy* 43, 131–144.

Sersic, J., 1963. Influence of the atmospheric and instrumental dispersion on the brightness distribution in a galaxy.

Simard, L., Willmer, C.N.A., Vogt, N.P., Sarajedini, V.L., Phillips, A.C., Weiner, B.J., Koo, D.C., Im, M., Illingworth, G.D., Faber, S.M., 2002. The deep groth strip survey ii. hubble space telescope structural parameters of galaxies in the groth strip. [astro-ph/0205025](#).

Simmons, B.D., Lintott, C., Willett, K.W., Masters, K.L., Kartaltepe, J.S., Häubler, B., Kaviraj, S., Krawczyk, C., Kruk, S.J., McIntosh, D.H., Smethurst, R.J., Nichol, R.C., Scarlata, C., Schawinski, K., Conselice, C.J., Almaini, O., Ferguson, H.C., Fortson, L., Hartley, W., Kocevski, D., Koekemoer, A.M., Mortlock, A., Newman, J.A., Bamford, S.P., Grogin, N.A., Lucas, R.A., Hathi, N.P., McGrath, E., Peth, M., Pforr, J., Rizer, Z., Wuyts, S., Barro, G., Bell, E.F., Castellano, M., Dahlen, T., Dekel, A., Ownsworth, J., Faber, S.M., Finkelstein, S.L., Fontana, A., Galametz, A., Grützbauch, R., Koo, D., Lotz, J., Mobasher, B., Mozena, M., Salvato, M., Wiklind, T., 2017. Galaxy Zoo: quantitative visual morphological classifications for 48 000 galaxies from CANDELS. *MNRAS* 464, 4420–4447. [1610.03070](#).

Simonyan, K., Zisserman, A., 2014. Very deep convolutional networks for large-scale image recognition. [1409.1556](#).

Skibba, R.A., Bamford, S.P., Nichol, R.C., Lintott, C.J., Andreescu, D., Edmondson, E.M., Murray, P., Raddick, M.J., Schawinski, K., Slosar, A., Szalay, A.S., Thomas, D., Vandenberg, J., 2009. Galaxy Zoo: disentangling the environmental dependence of morphology and colour. *MNRAS* 399, 966–982. [0811.3970](#).

Spergel, D., Gehrels, N., Breckinridge, J., Donahue, M., Dressler, A., Gaudi, B.S., Greene, T., Guyon, O., Hirata, C., Kalirai, J., Kasdin, N.J., Moos, W., Perlmutter, S., Postman, M., Rauscher, B., Rhodes, J., Wang, Y., Weinberg, D., Centrella, J., Traub, W., Baltay, C., Colbert, J., Bennett, D., Kiessling, A., Macintosh, B., Merten, J., Mortonson, M., Penny, M., Rozo, E., Savransky, D., Stapelfeldt, K., Zu, Y., Baker, C., Cheng, E., Content, D., Dooley, J., Foote, M., Goullioud, R., Grady, K., Jackson, C., Kruk, J., Levine, M., Melton, M., Peddie, C., Ruffa, J., Shaklan, S., 2013. Wide-Field InfraRed Survey Telescope-Astrophysics Focused Telescope Assets WFIRST-AFTA Final Report. *arXiv e-prints* , arXiv:1305.5422 [1305.5422](#).

Spindler, A., Geach, J.E., Smith, M.J., 2020. AstroVaDeR: Astronomical Variational Deep Embedder for Unsupervised Morphological Classification of Galaxies and Synthetic Image Generation. *arXiv e-prints* , arXiv:2009.08470 [2009.08470](#).

Tanoglidis, D., Ćiprijanović, A., Drlica-Wagner, A., 2020. DeepShadows: Separating Low Surface Brightness Galaxies from Artifacts using Deep Learning. *arXiv e-prints* , arXiv:2011.12437.

Tuccillo, D., Huertas-Company, M., Decencière, E., Velasco-Forero, S., 2017. Deep learning for studies of galaxy morphology, in: Brescia, M., Djorgovski, S.G., Feigelson, E.D., Longo, G., Cavaudi, S. (Eds.), *Astroinformatics*, pp. 191–196. [1701.05917](#).

Valle, R., Reda, F., Shoeybi, M., Legresley, P., Tao, A., Catanzaro, B., 2019. Neural odes for image segmentation with level sets. [1912.11683](#).

Willett, K.W., Galloway, M.A., Bamford, S.P., Lintott, C.J., Masters, K.L., Scarlata, C., Simmons, B.D., Beck, M., Cardamone, C.N., Cheung, E., Edmondson, E.M., Fortson, L.F., Griffith, R.L., Häubler, B., Han, A., Hart, R., Melvin, T., Parrish, M., Schawinski, K., Smethurst, R.J., Smith, A.M., 2017. Galaxy Zoo: morphological classifications for 120 000 galaxies in HST legacy imaging. *MNRAS* 464, 4176–4203. [1610.03068](#).

Willett, K.W., Lintott, C.J., Bamford, S.P., Masters, K.L., Simmons, B.D., Casteels, K.R.V., Edmondson, E.M., Fortson, L.F., Kaviraj, S., Keel, W.C., Melvin, T., Nichol, R.C., Raddick, M.J., Schawinski, K., Simpson, R.J., Skibba, R.A., Smith, A.M., Thomas, D., 2013. Galaxy Zoo 2: detailed morphological classifications for 304 122 galaxies from the Sloan Digital Sky Survey. *MNRAS* 435, 2835–2860. [1308.3496](#).

York, D.G., et al., 2000. The Sloan Digital Sky Survey: Technical Summary. *Astron. J.* 120, 1579–1587. [astro-ph/0006396](#).

Zhu, X.P., Dai, J.M., Bian, C.J., Chen, Y., Chen, S., Hu, C., 2019. Galaxy morphology classification with deep convolutional neural networks. *Ap&SS* 364, 55. [1807.10406](#).